

**Special Section:**Contributions from the  
Physics of Estuaries and  
Coastal Seas meeting, 2018**Key Points:**

- Processes impacting the German Bight stratification are investigated using a high-resolution baroclinic model
- The position of the river plume highly affects the contribution of tidal straining and mixing to changes in stratification
- Strong tidal straining can result in persistent stratification even during spring tides

**Correspondence to:**F. Chegini,  
fatemeh.chg@gmail.com**Citation:**Chegini, F., Holtermann, P., Kerimoglu, O., Becker, M., Kreuz, M., Klingbeil, K., et al. (2020). Processes of stratification and destratification during an extreme river discharge event in the German Bight ROFI. *Journal of Geophysical Research: Oceans*, 125, e2019JC015987. <https://doi.org/10.1029/2019JC015987>

Received 3 JAN 2020







Accepted 26 JUN 2020

Accepted article online 3 JUL 2020

©2020. The Authors.

This is an open access article under the terms of the Creative Commons Attribution License, which permits use, distribution and reproduction in any medium, provided the original work is properly cited.

# Processes of Stratification and Destratification During An Extreme River Discharge Event in the German Bight ROFI

Fatemeh Chegini<sup>1</sup> , Peter Holtermann<sup>1</sup> , Onur Kerimoglu<sup>2,3</sup> , Marius Becker<sup>4</sup>, Markus Kreuz<sup>5</sup>, Knut Klingbeil<sup>1</sup> , Ulf Gräwe<sup>1</sup> , Christian Winter<sup>4</sup>, and Hans Burchard<sup>1</sup> 

<sup>1</sup>Leibniz Institute for Baltic Sea Research Warnemünde (IOW), Rostock, Germany, <sup>2</sup>Institute for Coastal Research, Helmholtz-Zentrum Geesthacht, Geesthacht, Germany, <sup>3</sup>Institute for Chemistry and Biology of the Marine Environment, Carl von Ossietzky University Oldenburg, Oldenburg, Germany, <sup>4</sup>Institute of Geosciences, Christian-Albrechts-University, Kiel, Germany, <sup>5</sup>Federal Waterways Engineering and Research Institute, Hamburg, Germany

**Abstract** Processes of stratification and destratification in the German Bight region of fresh water influence (ROFI) are investigated following an extreme river discharge event in June 2013. For this purpose, a high-resolution baroclinic ocean model is set up and validated against field data. The model results are used to study the temporal and spatial variability of stratification and the duration of persistent stratification in 2013. The relevant processes affecting stratification are investigated by analyzing the potential energy anomaly budget, with a focus on mixing and tidal straining. It is shown that the stratification in the German Bight is highly affected by the spring-neap tidal cycle, with generally less stratification at spring tides due to dominant tidal mixing. It is also shown that the location of the river plume can modify this pattern. During spring tides, if the river plume is confined to the eastern region, stratification decreases significantly, as expected, due to the dominance of mixing over tidal straining. On the other hand, if the river plume moves toward deeper regions at spring tides, strong tidal straining becomes present. In this condition, mixing is weak, and the dominant tidal straining results in persistent stratification.

## 1. Introduction

Stratification plays a major role in the functioning of coastal ecosystems. Stratification affects vertical mixing and therefore impacts momentum, heat, and salt fluxes as well as other constituents such as suspended particulate matter (Pietrzak et al., 2011). Furthermore, the intensity of stratification impacts primary production by determining the amount of exposure of phytoplankton to average light and nutrient conditions (Peeters et al., 2013; Sharples et al., 2006), consequently affecting biogeochemical cycles. Therefore, understanding the processes of stratification and destratification is necessary for understanding the dynamics of coastal regions.

Coastal regions that are influenced by river outflow are referred to as regions of fresh water influence (ROFI). In a ROFI, the interaction between tides, wind, and freshwater buoyancy input determines the state of stratification on multiple time scales. On a tidal frequency, the water column condition can vary between fully mixed, stably stratified, and periodically stratified. The last condition is referred to as strain-induced periodic stratification (SIPS), a result of the stratifying and destratifying effect of the vertically sheared ebb and flood currents in the presence of a horizontal density gradient (Simpson et al., 1990). On a fortnightly time scale, the spring and neap tides can change the stratification of a ROFI. On a synoptic scale, the variability of the wind fields affect the state of stratification (Marques et al., 2010). The variability in river discharge influences the stratification on monthly to annual time scales (Marques et al., 2010). The amount of riverine discharge can vary considerably, especially at extreme precipitation events. During these events, the stratification of the region increases considerably, resulting in long-term, large-scale consequences on the coastal systems (Voynova et al., 2017). Therefore, understanding the processes that impact stratification during these events is essential for understanding the time scales of the extreme river discharge effects on coastal seas.

The processes of stratification and destratification can be investigated by analyzing the potential energy anomaly ( $\varphi$ ), a measure for stratification, introduced by Simpson et al. (1977). Burchard and Hofmeister

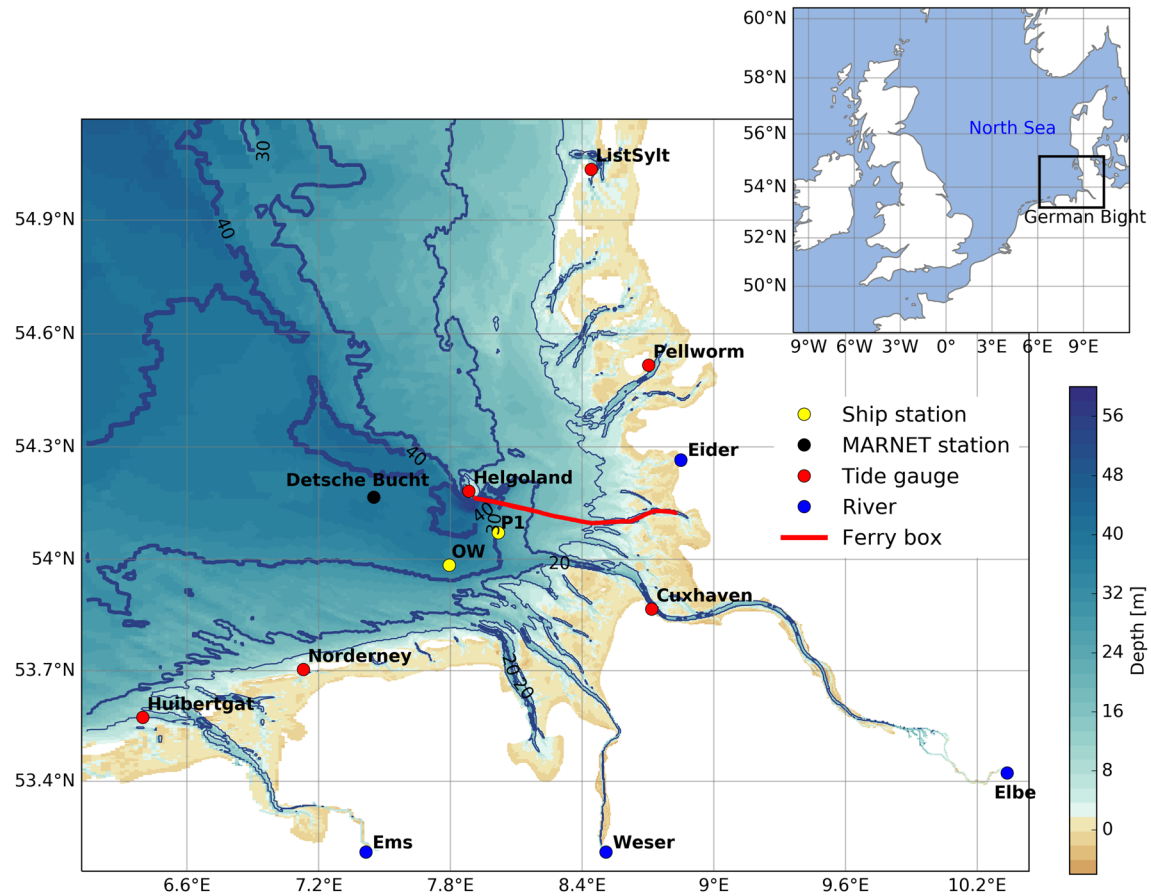


**Figure 1.** Model domain and bathymetry. Location of observational ship stations (yellow circles), MARNET station Deutsche Bucht (black circle), tide gauge stations (red circle), and rivers (blue circle). The transect route of the Funny Girl Ferry is shown by the red line. The 10 to 40 m isobaths are shown for every 10 m, with gradually increasing line width. Insert panel: The North Sea and the location of the German Bight.

(2008) derived a prognostic equation for  $\varphi$ , extending earlier formulations based on approximations (De Boer et al., 2008; Simpson & Bowers, 1981; van Aken, 1986). By means of these equations, the relative contributions of processes to stratification and destratification in coastal seas and estuaries were quantified on different time scales (De Boer et al., 2008; Hein, 2013; Hofmeister et al., 2009; Marques et al., 2010; Purkiani et al., 2015). These processes have been extensively studied in the Liverpool Bay and Rhine ROFIs (Howlett et al., 2011; Verspecht et al., 2009). However, despite its importance, these processes have not been studied in the German Bight (GB, see Figure 1).

The GB ROFI is a shallow region in the southern North Sea, with salinity values of 10 g/kg in near-coastal waters to 35 g/kg in the North Sea water (Becker et al., 1999). Several studies describe the circulation pattern and hydrodynamics of the GB using observational and numerical model data (Callies et al., 2017; Port et al., 2011; Stanev et al., 2016). The major rivers discharging into the GB are Elbe, Weser, Ems, and Eider. The annual mean discharge of these rivers in addition to the fraction of the Rhine waters passing the GB from west to north sum up to approximately 1,200 m<sup>3</sup>/s, making the GB a ROFI with medium runoff (Becker et al., 1999). The GB is exposed to strong vertical mixing due to tides and wind forcing. On the other hand, the freshwater supply to the GB has a strong tendency to increase vertical stratification. The competition between the mixing and the stratifying forces determines the degree of stratification of the region. Previous studies described the position of fronts in the GB and the related patterns of stratification. The frontal positions under different wind conditions were studied by Becker et al. (1992) and Dippner (1993). Frey (1990) showed that the stratification in the German Bight varies yearly. Schrum (1997) identified different stratification patterns depending on the wind direction and discussed some of the processes influencing

the mesoscale variability of stratification, including baroclinic instability and tidal stirring. However, these studies lack a systematic quantification of processes contributing to stratification and destratification in the GB. Furthermore, no study has investigated these processes under extreme river discharge.

In June 2013, large inflow of riverine waters from the Elbe and Weser estuaries discharged into the GB, with values exceeding 4,000 and 1,000 m<sup>3</sup>/s, which are well over the yearly mean climatological averages of about 750 and 250 m<sup>3</sup>/s, respectively. This event had persistent effects on stratification within the southeastern GB for more than 2 months after the peak of the extreme river discharge (Voynova et al., 2017). Despite the importance of the impact of this event, there have been limited studies on the influence of the extreme discharge on the GB ROFI system. Voynova et al. (2017) provided important insight on the impact of the event on the physical properties and biogeochemistry of the GB using observational data. Recently, Kerimoglu et al. (2020) studied the impact of the extreme event and the particular meteorological conditions on the physical and biogeochemical structure of the GB using a coupled biogeochemical-hydrodynamical model. However, there is still a need for a more detailed understanding of the temporal and spatial variability of the GB hydrodynamics under extreme river discharge events and the specific physical processes contributing to changes in stratification.

The present high-resolution model study has two objectives. The first objective is to investigate the effect of the 2013 extreme river discharge on the temporal and spatial variability of the GB hydrodynamics. This includes investigating (a) the duration and spatial extension of the stratification and (b) the effect of buoyancy, wind, and tidal forcing on the variability of stratification. The second objective is to quantify the physical processes that contribute to stratification and destratification in the GB under extreme river discharge events. To achieve the first objective, the  $\varphi$  fields calculated from the model results are analyzed. The second objective is achieved by calculating the relevant processes, using the dynamic equation for  $\varphi$  derived by Burchard and Hofmeister (2008).

## 2. Material and Methods

### 2.1. Numerical Model Description

The General Estuarine Transport Model (GETM Burchard & Bolding, 2002; Klingbeil & Burchard, 2013) has been used for the numerical simulations of the present study. Previously, GETM has been successfully applied to high-resolution modeling in the Wadden Sea (Duran-Matute et al., 2014; Gräwe et al., 2016; Purkiani et al., 2015), the Baltic Sea (Hofmeister et al., 2011; Holtermann et al., 2014), and the North Sea (Gräwe et al., 2015; van Leeuwen et al., 2015). GETM is a three-dimensional free-surface primitive equation model using the Boussinesq and boundary layer approximations. It is especially developed for applications in shallow coastal regions with substantial drying and flooding of intertidal flats (Klingbeil et al., 2018). The turbulence closure is implemented via the General Ocean Turbulence Model (GOTM; Umlauf et al., 2005). In this study, the vertical mixing was parameterized by means of a two-equation  $k$ - $\epsilon$  turbulence model. Advection of momentum and all scalar tracers in the horizontal was done by a third-order scheme (P2PDM; Pietrzak, 1998). In the vertical, a second-order TVD-scheme with Superbee limiter with reduced spurious mixing (Klingbeil et al., 2014) was applied. Time-stepping of the model is managed by explicit mode splitting (Klingbeil et al., 2018) with the baroclinic time step being a multiple of the barotropic time step. A wave model that accurately simulates surface waves is not included, but mixing due to wind waves is parameterized in GOTM.

The horizontal resolution of the curvilinear model grid gradually increases from 1,500 m at the western and northern open boundaries to 300 m in the inner GB (Figure 1). The model domain includes the Elbe estuary up to Geestacht weir as well as the Weser and Ems estuaries. It is understood that the 300 m resolution of the model is not sufficient to accurately resolve the complete dynamics inside the estuaries. In the vertical, 30 adaptive terrain-following layers (Hofmeister et al., 2010) were used with the adaption focusing on stratification, with the result that the vertical layer thickness is strongly reduced at high values of the buoyancy frequency. The lateral boundary data were taken from a three-dimensional model of the Southern North Sea (Gräwe et al., 2015). The boundary data include vertical profiles of salinity and temperature at a temporal resolution of 4 hr, as well as surface elevations and depth averaged velocity at a temporal resolution of 20 min. The applied open boundary conditions differ for each variable. The radiation scheme of Flather (1994) was applied for the elevations. For temperature and salinity, the flow relaxation scheme of

Martinsen and Engedahl (1987) with a four-cell-wide relaxation zone was applied. The initial conditions included temperature and salinity profiles which were also taken from the Southern North Sea model. The mode-splitting scheme was applied with a barotropic time step of 3 s and a baroclinic time step of 9 s for the summer months (June–August) and 15 s for the remaining months. The reason for using a lower time step during summer was the presence of strong stratification which increased the resolution of the vertical coordinate at the pycnocline. The model was run for the period 2010–2016. However, here only the simulation results of the year 2013 are analyzed with the exception of the model validation at the Stations P1 and OW, which was carried out for August 2016.

Meteorological forcing data were provided by the operational model of the German Weather Service Local Model (DWD-LM), with a horizontal resolution of approximately 7 km. These data include wind velocity and direction at 10 m above the sea surface, air temperature, and dew point temperature at 2 m above sea level, air pressure, precipitation, and total cloud cover with a temporal resolution of 3 hr. Air-sea fluxes of momentum, heat, and freshwater were calculated inside GETM by using the bulk formulae derived by Kondo (1975). The daily discharges of the four major rivers Elbe, Weser, Ems, and Eider were included. The river data were obtained from the German Bundesamt für Gewässerkunde with a daily resolution. The locations of the applied river discharge measurements were approximately 1 km upstream of the location of the model input discharge points. While GETM interpolates the meteorological forcing in time, the river discharges are kept constant until new data are provided.

## 2.2. Observations

Intertidal observations of velocities, temperature, salinity, and velocity shear microstructure were carried out at Stations P1 (54.06°N, 8.016°E) and OW (53.98°N, 7.79°E; see Figure 1). Although these two stations are located close to each other and at a similar distance offshore, they have different stratification conditions. Station P1 is affected by the Elbe river plume and therefore more stratified. However, the weaker Weser river plume does not generally reach the OW station, and therefore the water column at this station is usually mixed. At both stations, a rugged underwater frame was deployed before carrying out the profiling observations. An RDI Workhorse ADCP, in up-looking configuration Mode 1, with a frequency of 600 kHz was mounted on the frame, 2 m above the seafloor. The cell size was 0.25 m, and the time between ensembles was 3.2 s, recording averages of 4 subpings.

After the mooring was deployed, the ship was anchored and consecutive shear microstructure measurements were performed with a Sea & Sun Technology MSS-90L (MSS). Additional to a standard CTD package, the MSS was equipped with two PNS06 airfoil sensors (ISW, Germany). The buoyancy of the MSS was adjusted to achieve a falling speed of 0.8 m/s and was deployed from the ship by a loosely tethered cable. The data were recorded with 1,024 Hz and transmitted to an onboard computer. The data were saved and processed to derive the dissipation rate of turbulent kinetic energy ( $\epsilon$ ); for details of the processing algorithm, see Holtermann and Umlauf (2012). While on anchor, both wind and currents influenced the orientation of the ship. The ship swayed around the anchor location. As a result, no MSS measurements could be collected during slack water, in order to prevent the MSS cable to be entangled with the ship's propeller.

Another set of observational data is provided by a ship of opportunity, the Funny Girl Ferry, with a regular daily summer service between Helgoland Island and the coast (see Figure 1 for the ship track). The ship is equipped with a FerryBox system (Petersen et al., 2011) operated by the Helmholtz-Zentrum Geesthacht as part of the COSYNA coastal observatory (<https://www.cosyna.de>). In addition, temperature and salinity data obtained from the Deutsche Bucht station, part of the MARNET ([https://www.bsh.de/EN/DATA/data\\_node.html](https://www.bsh.de/EN/DATA/data_node.html)) measuring network that is operated by the German Federal Maritime and Hydrographic Agency (BSH), were used.

## 2.3. Potential Energy Anomaly

As a measure for stratification, the potential energy anomaly  $\varphi$  (Simpson & Bowers, 1981; Simpson et al., 1977) is defined as the amount of energy (per  $m^3$ ) required to homogenize the entire water column with a given density stratification:

$$\varphi = \frac{1}{D} \int_{-H}^{\eta} gz(\bar{\rho} - \rho) dz, \quad (1)$$

with the depth-averaged density

$$\bar{\rho} = \frac{1}{D} \int_{-H}^{\eta} \rho dz, \quad (2)$$

the mean water depth  $H$ , the sea surface elevation  $\eta$ , the actual water depth  $D = \eta + H$ , and the gravitational acceleration  $g$ . For a fully mixed water column,  $\varphi = 0$ . Positive  $\varphi$  values indicate stable stratification, and negative values represent unstable stratification. Based on the budget equations for temperature and salinity, Burchard and Hofmeister (2008) analytically derived a budget equation for  $\varphi$ :

$$\begin{aligned} \partial_t \varphi = & \underbrace{-\nabla_h(\bar{\mathbf{u}}\varphi)}_A + \underbrace{\frac{g}{D} \nabla_h \bar{\rho} \cdot \int_{-H}^{\eta} z \tilde{\mathbf{u}} dz}_B \\ & \underbrace{-\frac{g}{D} \int_{-H}^{\eta} \left(\eta - \frac{D}{2} - z\right) \tilde{\mathbf{u}} \cdot \nabla_h \tilde{\rho} dz}_C - \underbrace{\frac{g}{D} \int_{-H}^{\eta} \left(\eta - \frac{D}{2} - z\right) \tilde{w} \partial_z \tilde{\rho} dz}_D \\ & \underbrace{+\frac{\rho_0}{D} \int_{-H}^{\eta} P_b dz + F + G + H}_E, \end{aligned} \quad (3)$$

where  $\bar{\mathbf{u}}$  is the depth-averaged velocity,  $\tilde{\mathbf{u}} = \mathbf{u} - \bar{\mathbf{u}}$  is the deviation from the depth-averaged velocity, and  $\tilde{\rho}$  the deviation from the depth-averaged density.  $\tilde{w} = w - \bar{w}$  is the deviation from a linear vertical velocity profile  $\bar{w}$ , which would result from kinematic boundary conditions and the incompressibility condition as derived by Burchard and Hofmeister (2008).  $\nabla_h$  denotes the horizontal gradient operator, and  $P_b$  is the vertical buoyancy flux. In Equation 3, the left-hand side represents the temporal variation of  $\varphi$ . The right-hand side shows processes that contribute to local variations of  $\varphi$ . These processes include horizontal advection (A), depth mean straining (B), nonmean straining (C), vertical advection (D), vertical mixing (E), surface and bottom buoyancy fluxes (F), inner sources or sinks of potential density (G), and divergence of horizontal turbulent transport (H). For a more descriptive definition of each term and a sketch explaining how each term changes  $\varphi$ , see Burchard and Hofmeister (2008). The entire  $\varphi$  decomposition was done during runtime in GETM. Thus, truncation or discretization errors in the offline computation, as present by Purkiani et al. (2015), were avoided. The most important terms for the GB ROFI are the terms A–E, and therefore, only these terms are analyzed in this study. This was confirmed by comparing the time series of the sum of these terms to  $\partial_t \varphi$  at several points. Purkiani et al. (2015) have also shown that in a region that density is dominated by salinity, such as the GB, the terms A–E are sufficient to describe the changes in  $\varphi$ .

To achieve the two objectives of this study (detailed in section 1), different analyses based on  $\varphi$  were performed. The effect of extreme river discharge on the stratification is investigated by analyzing the temporal and spatial changes of  $\varphi$ . To cover the temporal variability of  $\varphi$  during a tidal cycle, hourly values were used. The duration of persistent stratification is calculated by considering the maximum number of days  $\varphi$  remains above a threshold value of  $10 \text{ J/m}^3$ . The analytical value of  $\varphi = 0 \text{ J/m}^3$  would detect the small density differences due to model round-off errors.  $\varphi = 10 \text{ J/m}^3$  approximately corresponds to the energy required to mix a 15 m deep water column with a density difference of  $0.7 \text{ kg/m}^3$  between the surface and bottom layer. This is also equivalent to approximately 5% of the maximum value of temporal mean of  $\varphi$  field calculated for June–August 2013. To evaluate the contribution of salinity ( $\varphi_S$ ) and temperature ( $\varphi_T$ ) to the  $\varphi$  values, a linear equation of state is used (Vallis, 2017):  $\rho = -\rho_T + \rho_S + \rho_p = \rho_0(-\alpha(T - T_0) + \beta(S - S_0) + \gamma(p - p_0))$  with  $\alpha = 0.17 \text{ K}^{-1}$  and  $\beta = 0.8 \text{ (g/kg)}^{-1}$ . To calculate  $\varphi_T$  and  $\varphi_S$ , the density term in Equation 1 is replaced by the temperature ( $\rho_T$ ) and salinity ( $\rho_S$ ) contribution to density, respectively.

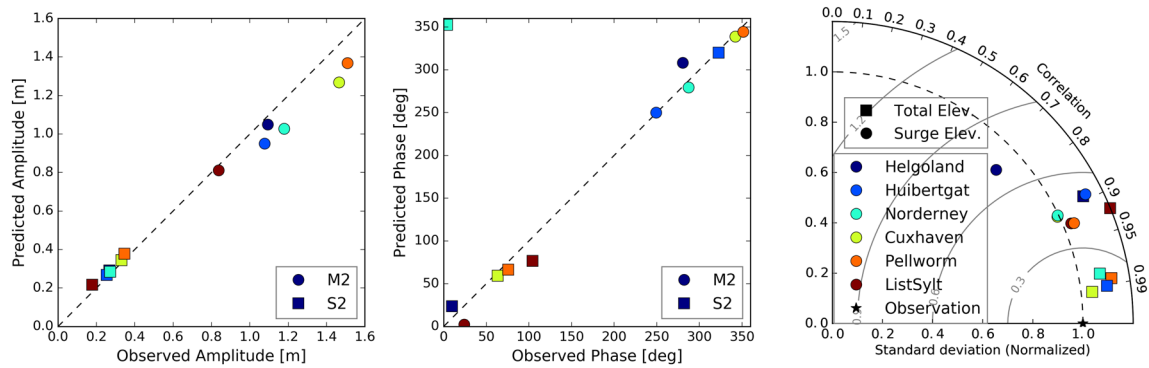


**Figure 2.** Validation of sea surface elevations. Left and middle: Comparison of simulated and observed amplitude and phase of the  $M_2$  and  $S_2$  tidal constituents at six monitoring stations. Right: Taylor diagram showing the the normalized standard deviation and the correlation between observed and simulated surge elevations.

The spatial distribution of the terms that control temporal changes in  $\varphi$  is evaluated using the covariance analysis (De Boer et al., 2008; Marques et al., 2010). The covariance between an arbitrary term  $\alpha$  in Equation 3 and the total derivative of  $\varphi$ ,  $D\varphi/Dt = \varphi_t + \nabla_h(\bar{\mathbf{u}}\varphi)$ , was calculated as

$$\text{cov}\left(\alpha, \frac{D\varphi}{Dt}\right) = \left\langle (\alpha - \langle\alpha\rangle) \left( \frac{D\varphi}{Dt} - \left\langle \frac{D\varphi}{Dt} \right\rangle \right) \right\rangle. \quad (4)$$

The angular brackets denote time averages. The reason for using the total derivative instead of the partial derivative was to eliminate the forward and backward advection of density structures due to the tidal movement (Hein, 2013).

The variability of stratification in the GB is evaluated by considering the spatial average of  $\varphi$  in the region during the 2013 extreme event. For this analysis, first the time average of  $\varphi$  over two  $M_2$  tidal cycles (about 25 hr) was calculated. Then the fraction of stratified region was calculated by defining stratified regions where  $\langle\varphi\rangle$  is larger than the small threshold value of  $10 \text{ J/m}^3$ . Finally, the cumulative effect of the different terms on the stratification of the region was assessed. For this analysis, the sum of the contribution of tidal straining (nonmean and depth-mean, i.e., B and C), advection (horizontal and vertical, i.e., A and D), and mixing (E) was calculated under different tidal and wind conditions.

### 3. Model Validation

#### 3.1. Tidal Propagation and Sea Surface Elevation

The main tidal constituents in the North Sea are the  $M_2$  and  $S_2$  constituents. Both semidiurnal lunar constituents propagate anticlockwise as a Kelvin-type wave through the North Sea. To assess the ability of the model in reproducing tides, classical harmonic analysis (Pawlowicz et al., 2002) was carried out for six tide gauge stations (locations shown in Figure 1). The model is able to properly reproduce the  $M_2$  and  $S_2$  tidal amplitudes and phases (Figure 2). The  $S_2$  tidal amplitudes are slightly overpredicted by the model, while the  $M_2$  amplitudes are underpredicted. However, the underprediction of the  $M_2$  tidal amplitude is very small for the reference station at Helgoland, while for the coastal gauges for which the model resolution of 300 m might not be sufficient are more severely underpredicted. The detided surge levels are moderately well simulated as shown by the Taylor diagram for the model skill assessment (Figure 2).

#### 3.2. Temperature and Salinity

The simulated salinity and temperature are qualitatively validated against observational data at the station *Deutsche Bucht* (see location in Figure 1). The model is able to reasonably well reproduce the surface (6 m) and bottom (30 m) temperature and salinity before, during, and after the extreme discharge event (Figure 3). The model reproduces the decrease in salinity during the extreme discharge event and the seasonal variation in temperature. However, the model slightly overpredicts the stratification, indicated by the difference between the surface and bottom salinity and temperature fields. This is probably due to the

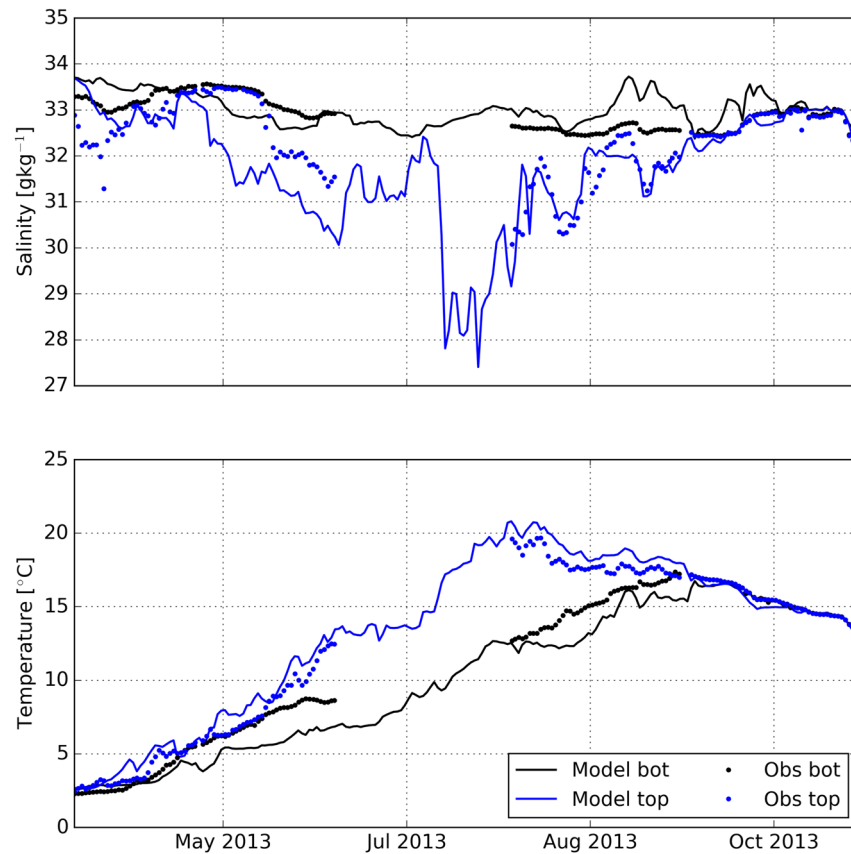


**Figure 3.** Comparison of observed and simulated surface (6 m) and bottom (30 m) salinity and temperature at the *Deutsche Bucht* station during the 2013 extreme discharge event.

underprediction of mixing by the model due to underprediction of the tidal amplitude. Possibly, it could have also been triggered by importing too strong stratification from the open boundary, a poor representation of the local bathymetry or an incorrect location of the simulated front.

The simulated horizontal salinity gradients are assessed next. Figure 4 shows the simulated sea surface salinity for May–October 2013 in comparison to observed FerryBox data. The model is able to reproduce the decrease in the surface salinity due the extreme river discharge, the spread of the freshwater plume offshore, and the flushing time of the freshwater. The horizontal salinity gradients referred from the difference between the coastal and offshore salinity fields are well reproduced by the model during the extreme event. In the nearshore, the surface salinity is slightly overpredicted, possibly due to underprediction of tidal mixing or insufficient representation of the Elbe estuarine dynamics as described in section 2.1. Furthermore, the model freshwater plume is more persistent compared to observations, resulting in a longer flushing time. Kerimoglu et al. (2020) have shown that these can be improved by extensive tuning of the horizontal diffusion.

### 3.3. Model Performance On A Tidal Cycle

The correct prediction of the changes in water column stratification during a tidal cycle is important in a ROFI region. The level of stratification and the frequency of change between stratified and mixed condition affects both the physical and biological properties of the region. To validate the model performance on a semidiurnal tidal frequency, the model results were assessed at the two stations P1 and OW with different water column stratification conditions. Simulated and observed profiles of current velocity, temperature, salinity, buoyancy frequency, and dissipation rates were compared. The current velocity was decomposed into major and minor tidal directions.

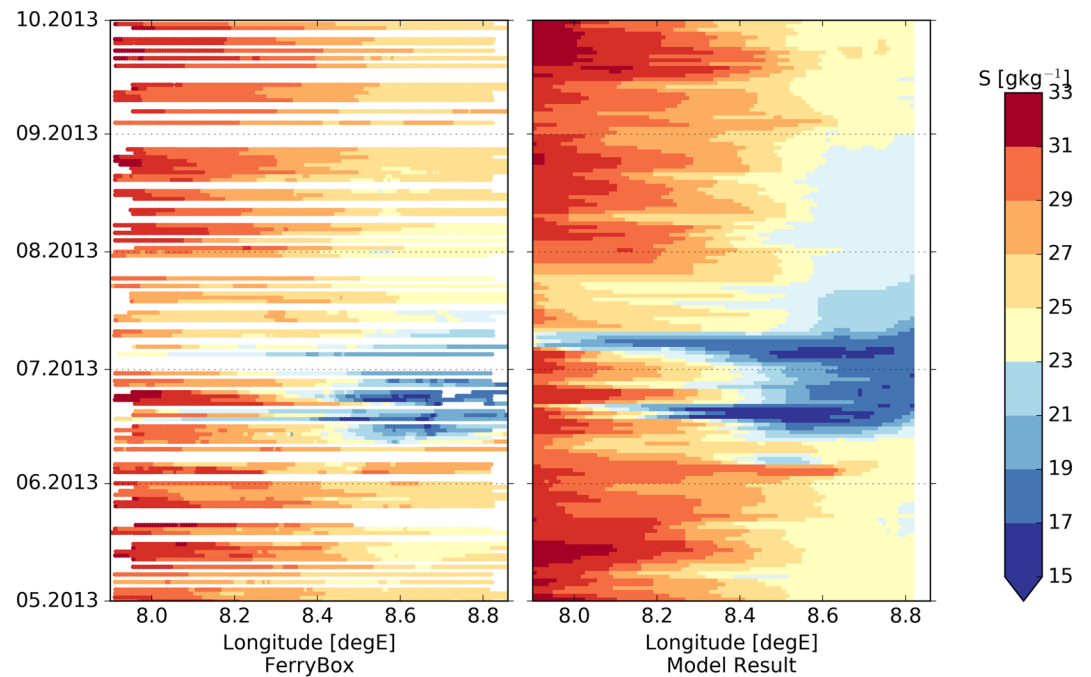


**Figure 4.** Comparison of observed (left) and simulated (right) sea surface salinity data during the 2013 extreme river discharge event along the Funny Girl FerryBox transect.

### 3.3.1. Station P1

Simulated velocity profiles at Station P1 are in good agreement with observations (Figure 5). During the observations, neap tide (beginning of spring tide) occurred with a depth-averaged tidal velocity amplitude of approximately 0.5 m/s. The velocity profiles in the major direction are well reproduced by the model with a maximum near-surface velocity of 0.9 m/s during maximum flood/ebb. In the minor direction, the model simulates a persistent northward velocity in the surface layer, in agreement with the observations. In the subsurface layer, both the observations and the model show velocity shear in the minor direction occurring at maximum ebb and persisting until maximum flood. The depth of the maximum shear occurred at 15 m in the observations but was underpredicted by the model. This velocity shear is due to the presence of stratification which modifies the vertical structure of the tidal ellipse characteristics (Souza & Simpson, 1996). The simulated salinity and temperature profiles are in good agreement with observations. Near the surface, a strongly stratified fresh and warm layer is persistent ( $\mathcal{O}(N^2) = 10^{-2} \text{ s}^{-2}$ ) through the entire tidal cycle. Below this layer, the water column is marginally stratified during ebb ( $\mathcal{O}(N^2) = 10^{-4} \text{ s}^{-2}$ ) and destratifies during flood, reaching minimum stratification at slack after flood. The depth of the near-surface persistent stratified layer is underpredicted in the model, which results in the underprediction of the depth of maximum shear in the minor direction. During the observation period, calm weather conditions were present. Therefore, the reason for the underprediction of the depth of the persistent fresh layer is not due to underprediction of surface stress from the wind/waves in the model. The difference between the model and observations is probably due to overprediction of the mixing by the tidal currents as observed from the comparison of dissipation rates.

Comparison of the dissipation rates shows a similar pattern in both the model data and observations. The turbulent dissipation rate shows an asymmetry between ebb and flood, in agreement with previous observations in a similar ROFI region (Simpson et al., 2002). During flood, the dissipation rate extends higher in the water column and up to the subsurface layer, inducing mixing and a vertical homogeneity below this layer. During ebb, the dissipation rate extends less in the water column, resulting in increased stratification. However, the model dissipation rate during the entire tidal cycle extends higher compared to the observations. This indicates a stronger bed stress in the model at Station P1 compared to observation. The dissipation rate in the bottom layer has an  $M_4$  component, with the maximum dissipation rate occurring during flood.



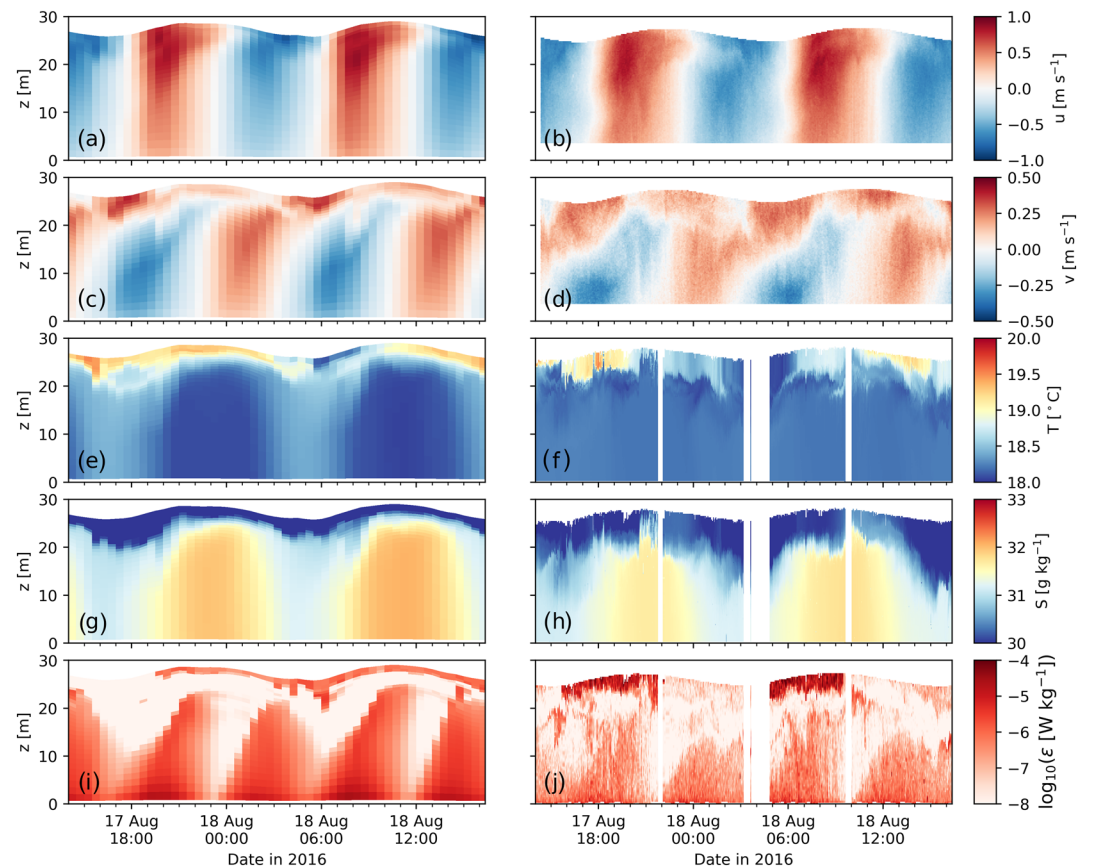


**Figure 5.** Comparison of simulated (a, c, e, g, i) and observed (b, d, f, h, j) currents in major (u) and minor (v) tidal direction, temperature, salinity, and dissipation rates at Station P1.

In the near surface layer, the maximum dissipation rate occurs at slack tide. For an explanation of the lag in turbulence production between the bottom and surface layers, refer to Souza et al. (2004).

### 3.3.2. Station OW

Simulated physical properties at Station OW are in good agreement with observations (Figure 6). Here, only the differences in model performance between the OW and P1 stations are described. Both the simulated and observed velocity profiles in the major and minor directions are more uniform during the entire tidal cycle compared to Station P1. This results in a lower velocity shear during slack after ebb at Station OW. The salinity and temperature profiles show that the water column at OW is vertically mixed during the entire tidal cycle in contrast to Station P1. The reason for this is that Station OW is less affected by the fresh water of the rivers compared to P1. The model results show slightly warmer and fresher water properties compared to observations. The dissipation rate at Station OW is higher than Station P1, but the pattern in the lower and upper layers are similar.

## 4. Results: Stratification in the GB During the Extreme River Discharge

Despite the unavoidable quantitative deviations between observations and model results shown in section 3, for example, the overprediction of stratification in the central GB in 2013 (see Figure 4) and the underprediction of stratification in the inner GB in 2016 (see Figures 5 and 6), the model can be assumed to obtain qualitatively correct and quantitatively approximate results. It should be noted that high-quality reproductions of water-column dynamics are relatively easily achievable when one-dimensional water-column models are locally calibrated; see, for example, Souza et al. (2008) and Verspecht et al. (2009). In a three-dimensional multiannual simulation, this is not possible to such a degree such that quantitative model errors need to be accepted, as long as they do not lead to qualitative errors.

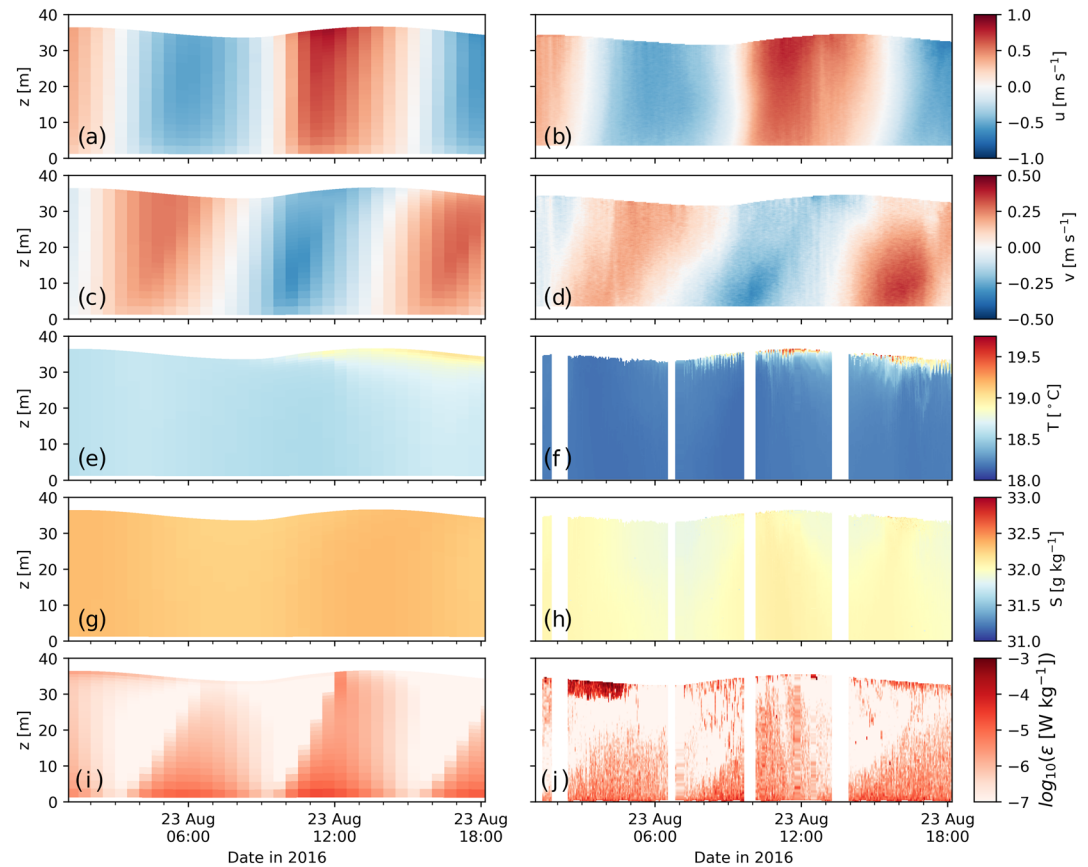


Figure 6. Same as Figure 5 but at Station OW.

#### 4.1. Duration of Stratification

To investigate the duration of stratification during 2013, the number of persistent stratified days for every grid point based on the method described in section 2 was calculated. The maximum number of persistent stratified days occurred at the deeper region of the Elbe paleo-valley (Figure 7). In the shallower southeastern and southwestern regions (with depths between 20 and 30 m), the duration of stratification varied between 40 and 120 days. In the intertidal region and at depths less than 5 m, no stratification was apparent. The temporal mean of  $\varphi$  field (calculated for the period June–August) shows that the maximum  $\varphi$  values occurred in the deeper region around Helgoland, peaking to  $170 \text{ J/m}^3$ . Comparison of the contribution of salinity and temperature ( $\varphi_S$  and  $\varphi_T$  as described in section 2) to  $\varphi$  shows that the stratification is mainly driven by vertical salinity gradients and modulated by vertical temperature gradients (Figures 7c and 7d).

#### 4.2. Temporal Variability of Stratification

Here, the variability of the stratification and spatially averaged salinity of the GB is investigated. To calculate the spatial average, the GB region (Figure 1) limited to  $53.4\text{--}54.9^\circ\text{N}$  and  $6.6\text{--}9^\circ\text{E}$  was considered, excluding areas shallower than 5 m and estuaries. To assess the effect of wind fields on the stratification, the spatially averaged wind was also calculated. The average wind condition during June was stronger than during July, with maximum wind stress being 0.25 and 0.15 Pa for June and July, respectively (Figure 8a). The average air temperature was  $13^\circ\text{C}$  in June and peaked to  $18^\circ\text{C}$  by beginning of August (not shown).

Before the extreme river discharge, the average salinity of the region was approximately 30 g/kg with the top and bottom mean salinity deviating by about 1 g/kg during neap tides (Figure 8). In early June, with increasing river discharge, the mean salinity started to decrease and dropped by about 1 g/kg by mid-June. After that, the mean salinity stayed constant for approximately 1 month and started to increase by mid-July. By the end of August, the mean salinity reached the normal values as before the extreme event. The mean

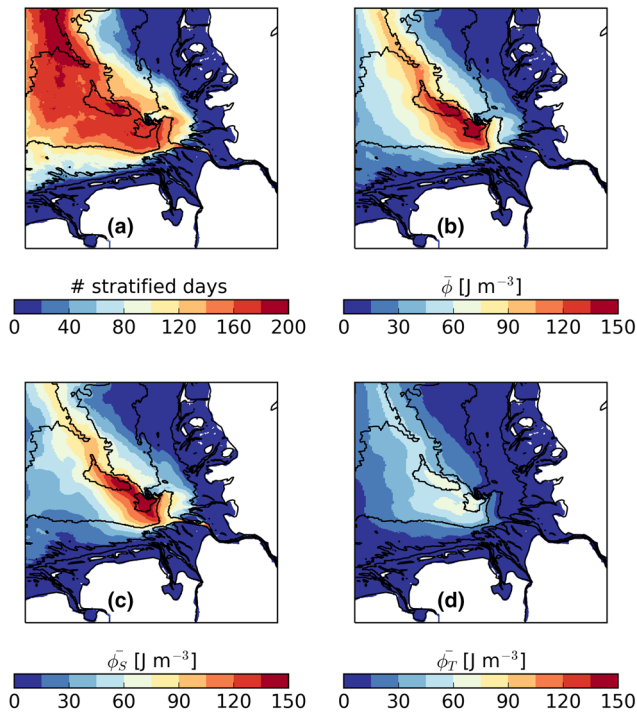


**Figure 7.** (a) Duration of persistent stratification (in days) from April–October 2013. (b) Temporal average of  $\bar{\phi}$  and the contribution of (c) salinity and (d) temperature to  $\bar{\phi}$  during June–August 2013.

surface and bottom layer salinity had similar patterns. However, the decrease in salinity was more pronounced in the surface than the bottom layers, leading to intensified stratification in the GB.

To assess the variability of the stratification in the GB before, during, and after the event, the fraction of stratified region from April to October is calculated based on the method described in section 2. The time series of the area fraction of the stratified region has a fortnightly frequency (Figure 8c), with minimum (maximum) stratification occurring during spring (neap) tides. Before the extreme event (April–June), approximately 50% of the region was stratified during neap tides and was reduced by 20% during spring tides. After the extreme river discharge, the fraction of stratified region during neap tides increased to about 60%. It should be noted that although the fraction of stratified region before and after the event is comparable, the region was less stratified before the event. That is a large area of low (high) stratification was present before (after) the event. During the first two spring tides after the event, the area fraction of the stratified region reduced by about 25%. However, from early July to mid-August, more than half of the region remained stratified. During this period of persistent stratified conditions, the fraction of stratified region during the third spring tide reduced by only 10%. The stratification returned to the normal values as before the event by mid-September.

In addition to tides, wind forcing affects the stratification in the GB. During the extreme river discharge event, the direction of the wind influenced the position of the salinity front, which affected the stratification.

The influence of the wind direction is evident by comparing the reduction in fraction of stratified region during spring tides. In the first phase (during the first and second spring tide, i.e., 8–15 June and 22–29 June), the stratified region reduced by more than 25%. During these periods, southwesterly winds constrained the river plume to the shallow regions of the eastern coast. In the second phase (during the third spring tide, i.e., 8–15 July), the stratified region decreased by only 10%. During this period, northerly winds moved the plume away from the shallow regions and toward the Elbe paleo-valley. This is consistent with previous studies showing that minimal stratification in the GB occurs during prevailing wind from southwest or south, while northeasterly winds induce the maximum extent of stratification (Schrum, 1997). This has been shown to be due to changes in circulation pattern of the GB. Furthermore, in their recent study, Kerimoglu et al. (2020) confirmed the effect of wind fields on the stratification of the GB during the 2013 extreme event, by simulating the hydrodynamics of the GB under different forcing scenarios. In the present study, a different approach is taken by evaluating the processes that contribute to the increase and decrease of stratification when the position of the river plume changes (section 4.3.1).

### 4.3. Analysis of the Potential Energy Anomaly Terms

#### 4.3.1. Cumulative Analysis

To evaluate the processes that affect the stratification in the GB during the extreme event, a cumulative analysis of the  $\bar{\phi}$  terms is carried out. The contribution of tidal straining, mixing, and advection is assessed. Tidal straining contribution is the sum of the depth-mean (Term B in Equation 3) and nonmean tidal straining (Term C). The advection contribution is the sum of the horizontal (Term A) and vertical advection (Term D). Positive (negative) values of each considered term increase (decrease)  $\bar{\phi}$ . When tidal straining is positive (negative), less dense (denser) water is sheared over denser (less dense) water, hence increasing (decreasing) stratification. The mixing term is positive (negative) in stable (unstable) stratification. When the water column is fully mixed, the mixing term is zero.

The analysis was carried out for three different periods: one period with increasing stratification during neap tide and two periods with decreasing stratification during spring tides. First, the period with increasing stratification (neap tide) between 30 June and 8 July is considered, when the fraction of stratified region

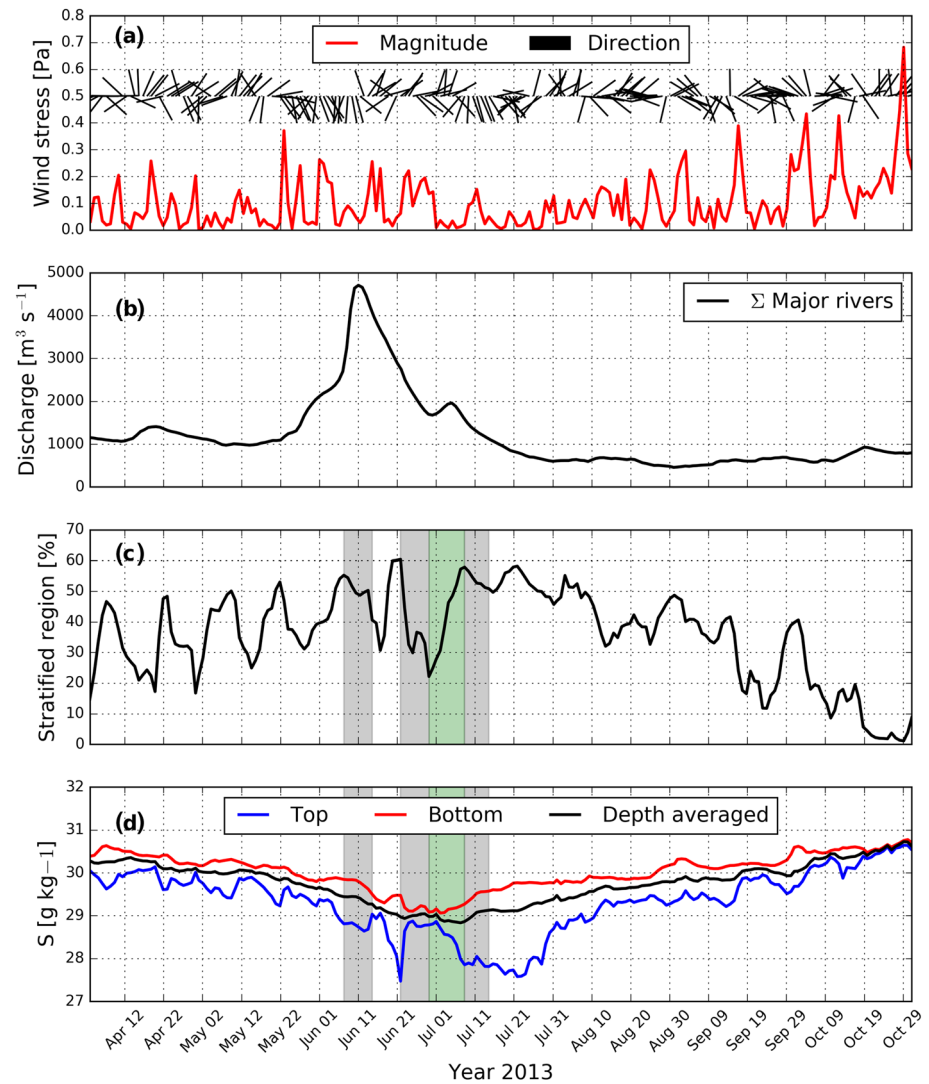


**Figure 8.** Variability of (a) wind stress and oceanographic direction, (b) total discharge of the four major rivers, (c) fraction of stratified region, and (d) spatially averaged top, bottom, and depth averaged salinity in the German Bight before, during, and after the 2013 extreme discharge event. The gray (green) areas in panels (c) and (d) show the spring (neap) tidal periods analyzed in sections 4.2 and 4.3.1.

increased by about 40%. During this period, the freshwater plume and salinity front were located in the eastern part of the region (Figure 9e). Tidal straining was positive in most of the region and maximum in the eastern part where a strong horizontal density gradient was present. The mixing term was also maximum in the eastern region except for shallow areas where it almost vanished. The small mixing term in these regions is due to the water column being mixed during the flood-ebb tide or the canceling of mixing in flood-ebb. Advection also contributed to the changes in stratification. However, in most areas, advection showed a patchy pattern and therefore did not systematically increase or decrease  $\varphi$ . In the entire GB, tidal straining exceeded mixing, resulting in increasing  $\varphi$ , specially in the southeast part of the GB.

The two periods with decreasing stratification during the second and third spring tide are analyzed next. First, the period 22–29 June, when the fraction of stratified region decreased by 30%, is considered. In this period, the river plume was constrained to the eastern coast of the GB (Figure 9j). The maximum horizontal density gradients, and hence the maximum tidal straining values, were also detected in this region. Tidal straining was positive along the eastern coast and around Helgoland. In these regions, strong mixing was

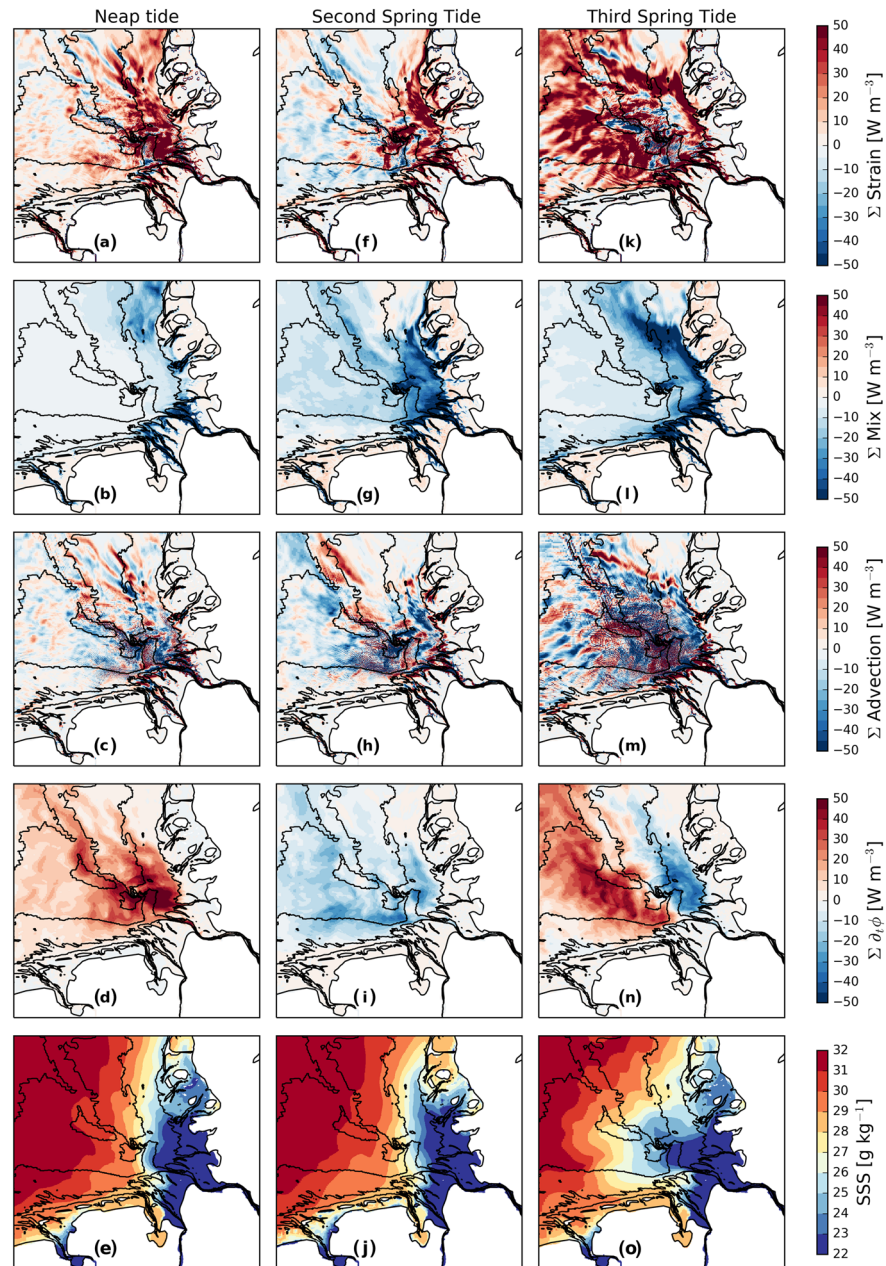


**Figure 9.** Total contribution of tidal straining: terms A+D, (first row: a, f, k), mixing: term E (second row: b, g, l), and advection: terms B+C (third row: c, h, m) to changes in  $\varphi$  during the neap tide, 30 June to 7 July (a–e), and two spring tides, that is, 22–29 June (f–j) and 8–15 July (k–o). Additionally, the total changes in  $\varphi$  during these periods (fourth row: d, i, n) and mean sea surface salinity (fifth row: e, j, o).

also present and dominated the tidal straining, resulting in the decrease of stratification. In the deeper region of the Elbe paleo-valley, the sum of tidal straining and advection was negative, adding to the effect of mixing on the decrease of  $\varphi$ . In total, during this period,  $\varphi$  decreased in the entire region.

Next the period between 7 and 14 July is analyzed, when the stratified region only decreased by 10%. The freshwater plume moved further toward Helgoland and the deeper regions of the GB in this period. Strong horizontal density gradients in most of the domain lead to strong positive tidal straining. Strong mixing was limited to the eastern region of the GB. Although mixing dominated tidal straining in the eastern region, tidal straining exceeded mixing in the deeper region of the Elbe paleo-valley. Therefore,  $\varphi$

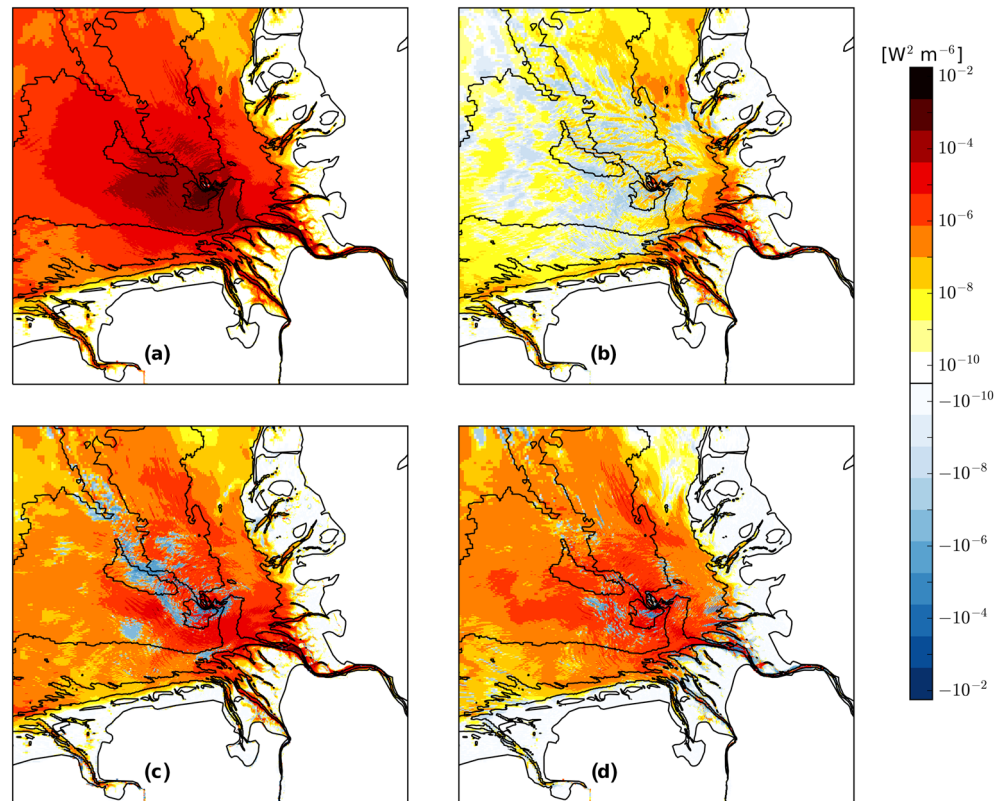


**Figure 10.** The covariance between the most important terms in Equation 3 and  $D\varphi/Dt$  as calculated from Equation 4. (a) Autocovariance of  $D\varphi/Dt$ ; other terms include (b) mixing, (c) depth-mean tidal straining, and (d) nonmean tidal straining.

decreased in the southeast region and increased in the deeper areas. This resulted in the fraction of stratified region slightly decreasing during this spring tide period.

#### 4.3.2. Covariance Analysis

The covariance is calculated between the total derivative of  $\varphi$  ( $D\varphi/Dt$ ) and three main terms in Equation 3: depth mean straining (B), nonmean straining (C), and mixing (E) using Equation 4 and for the period of three months during the extreme event: June–August. Here the nonmean and mean tidal straining are distinguished to investigate their separate contribution to changes in  $\varphi$ . Furthermore, the covariance is calculated for the sum of all significant terms ( $A+B+C+D+E$ ). The magnitude of the covariance depends on the product of  $D\varphi/Dt$  and the term under consideration (Equation 4). Therefore,  $D\varphi/Dt$  anomalies are stronger in regions where the covariance is high or the contribution of the considered term is important to the maintenance of the anomalies. As a means of comparison, the autocovariance of  $D\varphi/Dt$  can be used to identify regions where the  $D\varphi/Dt$  anomalies are large.

Analysis of the autocovariance values shows that the  $D\varphi/Dt$  anomalies are largest in the deep region west of Helgoland (Figure 10). This region approximately coincides with the region of maximum stratification (mean  $\varphi$ ) as shown in Figure 7b. In the shallow regions, the autocovariance is near zero, indicating that these regions are mostly mixed during the analysis period. The covariance between  $D\varphi/Dt$  and sum of all significant terms (not shown) are almost identical to the autocovariance field, confirming that these terms are sufficient to predict changes in  $\varphi$  in the GB.

In most of the region, the contribution of depth-mean tidal straining and nonmean tidal straining to the  $D\varphi/Dt$  anomalies is comparable and considerably more than the contribution of mixing. The tidal straining (both mean and nonmean) covariance is mostly positive, indicating that the changes in  $D\varphi/Dt$  and tidal straining terms have the same sign. The contribution of mixing is highest in the northeast and southeast region. In the northeast region, the high contribution of mixing in combination with the low contribution

of tidal straining resulted in low vertical density gradients (Figure 7b). In the deeper regions, the mixing covariance is low and mostly negative. The negative values are mainly a result of the increase of  $\varphi_t$  during the second spring tide as described in the previous section.

#### 4.4. Summary

A high-resolution baroclinic model was used to investigate the processes that affect the stratification of the GB following the 2013 extreme river discharge event. The model uses realistic meteorological and river forcing and is successfully validated against observational data. Although mixing due to wind waves is parameterized in the model, the exact simulation of surface waves is not included. It is understood that surface waves will influence stratification, especially in the outer part of the GB. This process, however, remains to be investigated and will be the subject of a subsequent analysis.

The model results were used to calculate the potential energy anomaly of the region as an indication for stratification. Furthermore, a dynamic equation for  $\varphi$  was applied to quantify the relevant processes that contribute to changes in stratification. Results showed that the maximum number of persistent stratified days occurred in the deeper region along the Elbe paleo-valley. In the shallower regions with depths between 20 and 30 m, the duration of stratification varied between 40 and 120 days. The maximum mean stratification during summer 2013 (June–August) occurred near Helgoland. Furthermore, it was shown that the stratification of the region was mainly due to salinity gradients.

Analysis of the temporal variability of the fraction of stratified region showed that the stratification in the GB is highly affected by the spring-neap cycle. Furthermore, the position of the river plume affects the changes in stratification during this cycle. During the extreme river discharge, the position of the plume varied between being confined to the eastern coastal region to extending toward offshore deeper regions. This variability was shown both by the model and the FerryBox observations. The extension of the plume toward deeper regions lead to persistent stratification during spring tides. Analysis of the  $\varphi$  terms showed that this was due to dominance of strong tidal straining over low mixing in the deep regions. To further confirm the effect of the river plume due to changes in wind direction, a scenario run without local winds was carried out (not shown). Results showed that in the absence of local winds, the pattern of the time series of fraction of stratified region is more regular with about 25% decrease (increase) during spring (neap) tides.

This study provides insight to the processes of stratification and destratification during an extreme river discharge event and the effects of the event on the physical properties of a coastal system. The results of this study can be used to understand the effect of such events, which are expected to become more frequent with changes in climate (Christensen & Christensen, 2004), on similar ROFI regions such as the Liverpool Bay for future risk managements.

#### Data Availability Statement

Details on obtaining the open-source GETM model are described at <https://getm.eu/software.html>. The FerryBox and MARNET data are available from <https://www.cosyna.de> and [https://www.bsh.de/EN/DATA/data\\_node.html](https://www.bsh.de/EN/DATA/data_node.html), respectively. The ADCP observational data at Stations P1 and OW can be obtained from <https://doi.org/10.1594/PANGAEA.919168>. The MSS measurements and the model data are available at <https://doi.io-warnemuende.de/10.12754/data-2020-0004>.

#### References

- Becker, G. A., Dick, S., & Dippner, J. W. (1992). Hydrography of the German Bight. *Marine Ecology Progress Series*, 91, 9–18.
- Becker, G. A., Giese, H., Isert, K., König, P., Langenberg, H., Pohlmann, T., & Schrum, C. (1999). Mesoscale structures, fluxes and water mass variability in the German Bight as exemplified in the KUSTOS-experiments and numerical models. *Deutsche Hydrografische Zeitschrift*, 51(2-3), 155–179.
- Burchard, H., & Bolding, K. (2002). *GETM: A general estuarine transport model; Scientific documentation*. European Commission, Joint Research Centre, Institute for Environment and Sustainability.
- Burchard, H., & Hofmeister, R. (2008). A dynamic equation for the potential energy anomaly for analysing mixing and stratification in estuaries and coastal seas. *Estuarine, Coastal and Shelf Science*, 77(4), 679–687. <https://doi.org/10.1016/j.ecss.2007.10.025>
- Callies, U., Gaslikova, L., Kapitza, H., & Scharfe, M. (2017). German Bight residual current variability on a daily basis: Principal components of multi-decadal barotropic simulations. *Geo-Marine Letters*, 37(2), 151–162.
- Christensen, O. B., & Christensen, J. H. (2004). Intensification of extreme European summer precipitation in a warmer climate. *Global and Planetary Change*, 44(1-4), 107–117. <https://doi.org/10.1016/j.gloplacha.2004.06.013>

#### Acknowledgments

The authors would like to thank Arne Hamrich for discussions on the analysis of tidal data and Yoana G. Voynova for the processing of the FerryBox data. We also thank A. Souza and an anonymous reviewer for their constructive comments on the original manuscript. Support has been granted by the project MOSSCO (Modular System for Shelves and Coasts) funded by the German Federal Ministry of Research and Education (BMBF) under the Project Identification Number FKZ 03F0740B. The work was further supported by the Morphodynamic Response of the Wadden Sea to Climate Change (MOREWACC) project funded by the German Research Foundation as BU 1199/21-1 under the umbrella of Priority Program SPP 1889 on Regional Sea Level Change and Society. O. K. was supported by the German Environment Agency, UBA, with Grant Number 3718252110. K. K. acknowledges the financial support by the Collaborative Research Centre TRK 181 on Energy Transfer in Atmosphere and Ocean (Project 274762653) funded by the German Research Foundation. The simulations were run on the Norddeutsche Verbund für Hoch und Höchstleistungsrechnen (HLRN) high-performance computing system.

- De Boer, G. J., Pietrzak, J. D., & Winterwerp, J. C. (2008). Using the potential energy anomaly equation to investigate tidal straining and advection of stratification in a region of freshwater influence. *Ocean Modelling*, *22*(1-2), 1–11. <https://doi.org/10.1016/j.ocemod.2007.12.003>
- Dippner, J. W. (1993). A frontal-resolving model for the German Bight. *Continental Shelf Research*, *13*(1), 49–66.
- Duran-Matute, M., Gerkema, T., De Boer, G. J., Nauw, J. J., & Gräwe, U. (2014). Residual circulation and freshwater transport in the Dutch Wadden Sea: A numerical modelling study. *Ocean Science*, *10*(4), 611–632. <https://doi.org/10.5194/os-10-611-2014>
- Flather, R. A. (1994). A storm surge prediction model for the northern Bay of Bengal with application to the cyclone disaster in April 1991. *Journal of Physical Oceanography*, *24*(1), 172–190.
- Frey, H. (1990). Stratification during periods of oxygen deficiency in the German Bight during the summers from 1981 to 1983: A comparison with the long-term variation in stratification. *Meeresforschung MEERD*, *32*(4).
- Gräwe, U., Flöser, G., Gerkema, T., Duran-Matute, M., Badewien, T. H., Schulz, E., & Burchard, H. (2016). A numerical model for the entire Wadden Sea: Skill assessment and analysis of hydrodynamics. *Journal of Geophysical Research: Oceans*, *121*, 5231–5251. <https://doi.org/10.1002/2016JC011655>
- Gräwe, U., Holtermann, P., Klingbeil, K., & Burchard, H. (2015). Advantages of vertically adaptive coordinates in numerical models of stratified shelf seas. *Ocean Modelling*, *92*, 56–68. <https://doi.org/10.1016/j.ocemod.2015.05.008>
- Hein, B. (2013). Processes of stratification and destratification in the Mekong ROFI-seasonal and intraseasonal variability (Ph.D. thesis). <https://ediss.sub.uni-hamburg.de/volltexte/2013/6369/>
- Hofmeister, R., Beckers, J.-M., & Burchard, H. (2011). Realistic modelling of the exceptional inflows into the central Baltic Sea in 2003 using terrain-following coordinates. *Ocean Modelling*, *39*(3), 233–247.
- Hofmeister, R., Burchard, H., & Beckers, J.-M. (2010). Non-uniform adaptive vertical grids for 3D numerical ocean models. *Ocean Modelling*, *33*, 70–86.
- Hofmeister, R., Burchard, H., & Bolding, K. (2009). A three-dimensional model study on processes of stratification and de-stratification in the Limfjord. *Continental Shelf Research*, *29*(11-12), 1515–1524.
- Holtermann, P. L., Burchard, H., Gräwe, U., Klingbeil, K., & Umlauf, L. (2014). Deep-water dynamics and boundary mixing in a nontidal stratified basin: A modeling study of the Baltic Sea. *Journal of Geophysical Research: Oceans*, *119*, 1465–1487. <https://doi.org/10.1002/2013JC009483>
- Holtermann, P. L., & Umlauf, L. (2012). The Baltic Sea tracer release experiment: 2. Mixing processes. *Journal of Geophysical Research*, *117*, C01022. <https://doi.org/10.1029/2011JC007445>
- Howlett, E. R., Rippeth, T. P., & Howarth, J. (2011). Processes contributing to the evolution and destruction of stratification in the Liverpool Bay ROFI. *Ocean Dynamics*, *61*(9), 1403–1419.
- Kerimoglu, O., Voynova, Y. G., Chegini, F., Brix, H., Callies, U., Hofmeister, R., et al. (2020). Interactive impacts of meteorological and hydrological conditions on the physical and biogeochemical structure of a coastal system. *Biogeosciences*. <https://doi.org/10.5194/bg-2020-1>
- Klingbeil, K., & Burchard, H. (2013). Implementation of a direct nonhydrostatic pressure gradient discretisation into a layered ocean model. *Ocean Modelling*, *65*, 64–77. <https://doi.org/10.1016/j.ocemod.2013.02.002>
- Klingbeil, K., Lemarié, F., Debreu, L., & Burchard, H. (2018). The numerics of hydrostatic structured-grid coastal ocean models: State of the art and future perspectives. *Ocean Modelling*, *125*, 80–105. <https://doi.org/10.1016/j.ocemod.2018.01.007>
- Klingbeil, K., Mohammadi-Aragh, M., Gräwe, U., & Burchard, H. (2014). Quantification of spurious dissipation and mixing—Discrete variance decay in a finite-volume framework. *Ocean Modelling*, *81*, 49–64. <https://doi.org/10.1016/j.ocemod.2014.06.001>
- Kondo, J. (1975). Air-sea bulk transfer coefficients in diabatic conditions. *Boundary-Layer Meteorology*, *9*(1), 91–112.
- Marques, W. C., Fernandes, E. H. L., & Moller, O. O. (2010). Straining and advection contributions to the mixing process of the Patos Lagoon coastal plume, Brazil. *Journal of Geophysical Research*, *115*, C06019. <https://doi.org/10.1029/2009JC005653>
- Martinsen, E. A., & Engedahl, H. (1987). Implementation and testing of a lateral boundary scheme as an open boundary condition in a barotropic ocean model. *Coastal Engineering*, *11*, 603–627. [https://doi.org/10.1016/0378-3839\(87\)90028-7](https://doi.org/10.1016/0378-3839(87)90028-7)
- Pawlowicz, R., Beardsley, B., & Lentz, S. (2002). Classical tidal harmonic analysis including error estimates in MATLAB using T\_TIDE. *Computers & Geosciences*, *28*(8), 929–937.
- Peeters, F., Kerimoglu, O., & Straile, D. (2013). Implications of seasonal mixing for phytoplankton production and bloom development. *Theoretical Ecology*, *6*(2), 115–129. <https://doi.org/10.1007/s12080-012-0164-2>
- Petersen, W., Schroeder, F., & Bockelmann, F.-D. (2011). FerryBox - Application of continuous water quality observations along transects in the North Sea. *Ocean Dynamics*, *61*(10), 1541–1554. <https://doi.org/10.1007/s10236-011-0445-0>
- Pietrzak, J. (1998). The use of TVD limiters for forward-in-time upstream-biased advection schemes in ocean modeling. *Monthly Weather Review*, *126*(3), 812–830.
- Pietrzak, J. D., de Boer, G. J., & Eleveld, M. A. (2011). Mechanisms controlling the intra-annual mesoscale variability of SST and SPM in the southern North Sea. *Continental Shelf Research*, *31*(6), 594–610. <https://doi.org/10.1016/j.csr.2010.12.014>
- Port, A., Gurgel, K.-W., Staneva, J., Schulz-Stellenfleth, J., & Stanev, E. V. (2011). Tidal and wind-driven surface currents in the German Bight: HFR observations versus model simulations. *Ocean Dynamics*, *61*(10), 1567–1585.
- Purkiani, K., Becherer, J., Flöser, G., Gräwe, U., Mohrholz, V., Schuttelaars, H. M., & Burchard, H. (2015). Numerical analysis of stratification and destratification processes in a tidally energetic inlet with an ebb tidal delta. *Journal of Geophysical Research: Oceans*, *120*, 225–243. <https://doi.org/10.1002/2014JC010325>
- Schrum, C. (1997). Thermohaline stratification and instabilities at tidal mixing fronts: Results of an eddy resolving model for the German Bight. *Continental Shelf Research*, *17*(6), 689–716.
- Sharples, J., Ross, O. N., Scott, B. E., Greenstreet, S. P. R., & Fraser, H. (2006). Inter-annual variability in the timing of stratification and the spring bloom in the north-western North Sea. *Continental Shelf Research*, *26*(6), 733–751. <https://doi.org/10.1016/j.csr.2006.01.011>
- Simpson, J. H., & Bowers, D. (1981). Models of stratification and frontal movement in shelf seas. *Deep Sea Research Part A. Oceanographic Research Papers*, *28*(7), 727–738.
- Simpson, J. H., Brown, J., Matthews, J., & Allen, G. (1990). Tidal straining, density currents, and stirring in the control of estuarine stratification. *Estuaries*, *13*(2), 125–132.
- Simpson, J. H., Burchard, H., Fisher, N. R., & Rippeth, T. P. (2002). The semi-diurnal cycle of dissipation in a ROFI: Model-measurement comparisons. *Continental Shelf Research*, *11*(22), 1615–1628.
- Simpson, J. H., Hughes, D. G., & Morris, N. C. G. (1977). The relation of seasonal stratification to tidal mixing on the continental shelf. A voyage of discovery.



- Souza, A. J., Alvarez, L. G., & Dickey, T. D. (2004). Tidally induced turbulence and suspended sediment. *Geophysical Research Letters*, *31*, L20309. <https://doi.org/10.1029/2004GL021186>
- Souza, A. J., & Simpson, J. H. (1996). The modification of tidal ellipses by stratification in the Rhine ROFI. *Continental Shelf Research*, *16*(8), 997–1007.
- Stanev, E. V., Schulz-Stellenfleth, J., Staneva, J., Grayek, S., Grashorn, S., Behrens, A., et al. (2016). Ocean forecasting for the German Bight: From regional to coastal scales. *Ocean Science*, *12*(5), 1105.
- Umlauf, L., Burchard, H., & Bolding, K. (2005). General ocean turbulence model. Source code documentation. *Baltic Sea Research Institute Warnemünde Technical Report*, *63*, 346.
- Vallis, G. K. (2017). *Atmospheric and oceanic fluid dynamics*. Cambridge University Press.
- van Aken, H. M. (1986). The onset of seasonal stratification in shelf seas due to differential advection in the presence of a salinity gradient. *Continental Shelf Research*, *5*(4), 475–485.
- van Leeuwen, S., Tett, P., Mills, D., & van der Molen, J. (2015). Stratified and nonstratified areas in the North Sea: Long-term variability and biological and policy implications. *Journal of Geophysical Research: Oceans*, *120*, 4670–4686. <https://doi.org/10.1002/2014JC010485>
- Verspecht, F., Rippeth, T. P., Howarth, M. J., Souza, A. J., Simpson, J. H., & Burchard, H. (2009). Processes impacting on stratification in a region of freshwater influence: Application to Liverpool Bay. *Journal of Geophysical Research*, *114*, C11022. <https://doi.org/10.1029/2009JC005475>
- Voynova, Y. G., Brix, H., Petersen, W., Weigelt-Krenz, S., & Scharfe, M. (2017). Extreme flood impact on estuarine and coastal biogeochemistry: the 2013 Elbe flood. *Biogeosciences*, *14*(3), 541.